Nanotoxicology, March 2013; 7(2):157–168

ISSN: 1743-5390 print / 1743-5404 online
DOI: 10.3109/17435390.2011.647929

informa
healthcare

Reactive oxygen species-mediated p38 MAPK regulates carbon nanotube-induced fibrogenic and angiogenic responses

Neelam Azad[1], Anand Krishnan V. Iyer[1], Liying Wang[2], Yuxin Liu[3], Yongju Lu[4], & Yon Rojanasakul[4]

[1]*Department of Pharmaceutical Sciences, Hampton University, Hampton, VA, USA,* [2]*National Institute for Occupational Safety and Health, Pathology and Physiology Research Branch, Morgantown, WV, USA,* [3]*Department of Computer Science and Electrical Engineering, West Virginia University, Morgantown, WV, USA and* [4]*Department of Pharmaceutical Sciences, West Virginia University, Morgantown, WV, USA*

Abstract

Single-walled carbon nanotubes (SWCNTs) are fibrous nanoparticles that are being used widely for various applications including drug delivery. SWCNTs are currently under special attention for possible cytotoxicity. Recent reports suggest that exposure to nanoparticles leads to pulmonary fibrosis. We report that SWCNT-mediated interplay of fibrogenic and angiogenic regulators leads to increased angiogenesis, which is a novel finding that furthers the understanding of SWCNT-induced cytotoxicity. SWCNTs induce fibrogenesis through reactive oxygen species-regulated phosphorylation of p38 mitogen-activated protein kinase (MAPK). Activation of p38 MAPK by SWCNTs led to the induction of transforming growth factor (TGF)-β1 as well as vascular endothelial growth factor (VEGF). Both TGF-β1 and VEGF contributed significantly to the fibroproliferative and collagen-inducing effects of SWCNTs. Interestingly, a positive feedback loop was observed between TGF-β1 and VEGF. This interplay of fibrogenic and angiogenic mediators led to increased angiogenesis in response to SWCNTs. Overall this study reveals key signalling molecules involved in SWCNT-induced fibrogenesis and angiogenesis.

Keywords: SWCNTs, angiogenesis, p38 MAPK, TGF-β1, VEGF

Introduction

Nanotechnology is revolutionising various fields by presenting enormous opportunities to create new and better products. Single-walled carbon nanotubes (SWCNTs) have enjoyed an exponential growth in utility, mainly in areas dealing with electronics, computers and drug delivery. With these applications come unprecedented avenues of human exposure to nanoparticles. The potential risks to human health from inhalation of SWCNTs are due to their small particle size. Carbon nanotubes have the ability to escape phagocytosis, cross cell membranes, pass the blood–brain barrier and redistribute to other sites of the body causing systemic side effects (Oberdorster et al. 2005; Shvedova & Kagan 2010). Inhaled SWCNTs typically end up in the interstitial compartment of the lung, either between or inside the cells, making up the alveolar wall. Once in the lung, the clearance rate of the nanomaterials is extremely low, leading to bio-persistence and tissue burden, resulting in a higher probability of an adverse response (Lam et al. 2004). Various *in vivo* studies on pulmonary exposure of SWCNTs suggest that these nanoparticles induce an inflammatory response leading to the development of granulomas and transportation to the pleura and extrapulmonary locations leading to pulmonary fibrosis (Shvedova et al. 2005; Warheit et al. 2004; Shvedova et al. 2008).

Pulmonary fibrosis is a progressive and lethal lung disease characterised by excessive proliferation of fibroblasts and deposition of extracellular matrix (ECM) (Crouch 1990; Thannickal et al. 2004; Lu et al. 2010). Elaboration of a provisional ECM by fibroblasts is an early repair function that aids epithelial cell migration and regeneration to restore barrier functions and maintain tissue architecture mirroring wound-healing process (Clark et al. 1986). Transforming growth factor (TGF)-β1 is essential for wound healing and has been implicated in the pathogenesis of pulmonary fibrosis (Kang et al. 2007). Overexpression of TGF-β1 in lungs from patients with pulmonary fibrosis has been extensively reported (Daniels et al. 2004; Khalil et al. 2001; Xu et al. 2003). In addition to its pro-fibrotic activity, TGF-β1 is also demonstrated to have pro-angiogenic effects (Roberts et al. 1986; Yang & Moses 1990). The existence of angiogenesis in pulmonary fibrosis was first identified by Turner-Warwick, who demonstrated neovascularisation leading to anastomoses between the systemic and pulmonary microvasculature of patients with widespread pulmonary fibrosis (Turner-Warwick 1963). Various other reports have demonstrated

Correspondence: Neelam Azad, Department of Pharmaceutical Sciences, Hampton University, Hampton, VA 23668, USA. Tel: +757 637 2539. Fax: +757 727 5840. E-mail: neelam.azad@hamptonu.edu

(Received 11 June 2011; accepted 1 November 2011)

vascular remodelling in pulmonary fibrosis suggesting that neovascularisation enhances fibrosis (Peao et al. 1994, Cosgrove et al. 2004, Renzoni et al. 2003). Furthermore, studies using both animal models and tissue specimens from patients with pulmonary fibrosis suggest an imbalance in the levels of angiogenic chemokines as compared with angiostatic chemokines, favouring net angiogenesis (Keane et al. 1997; Keane et al. 1999a; Keane et al. 2001; Keane et al. 1999b). However, the role of the central angiogenic regulator vascular endothelial growth factor (VEGF) in pulmonary fibrosis is largely unknown. VEGF plays an important role in vascular permeability and angiogenesis by inducing migration, proliferation, elongation, network formation and branching of endothelial cells (Carmeliet 2000; Helmlinger et al. 2000). In normal adult human lung, VEGF is expressed abundantly by various cells including alveolar epithelial cells, Clara cells, macrophages and fibroblasts (Fehrenbach et al. 1999). It is also reported to be abnormally regulated in patients with fibrotic diseases including idiopathic myelofibrosis (Steurer et al. 2007) and diffuse lung fibrosis (Meyer et al. 2000).

Various cell survival pathways have been widely reported to play a critical role in cell growth, angiogenesis and tumorigenesis. However, their involvement in the fibrotic process and the underlying mechanism is largely unclear. The mitogen-activated protein kinase (MAPK)-mediated signal transduction pathways are major pathways by which extracellular stimuli are transmitted to the intracellular signal. The p38 MAPKs are members of the MAPK family that are activated by variety of environmental stresses and inflammatory cytokines including oxidative stress, osmotic stress, ultraviolet irradiation, lipopolysaccharide, proinflammatory cytokines and DNA-damaging agents (Beyaert et al. 1996; Han et al. 1994; Iordanov et al. 1997; Moriguchi et al. 1996; Pandey et al. 1996; Raingeaud et al. 1995). In the present study, the interplay of oxidative, angiogenic and fibrotic mediators in response to SWCNT exposure was investigated. We used genetic and pharmacological approaches to study the involvement of signalling transduction pathways and studied their effect on SWCNT-induced fibrogenesis. SWCNT-induced fibrogenic effects were dependent on reactive oxygen species (ROS) generation. The p38 MAPK is the major cell survival pathway involved in the fibroproliferative and collagen-inducing effects of SWCNTs, and these effects are mediated in part through TGF-β1 and VEGF activation. ROS-dependent p38 MAPK-mediated induction of TGF-β1 and VEGF in response to SWCNTs exposure also led to angiogenesis suggesting a close association between SWCNT-induced fibrogenesis and angiogenesis.

Materials and methods

Preparation of SWCNTs

Nanoparticles (SWCNTs) used in this study are the same as published by our group previously (Wang et al. 2010a). The aforementioned article describes in detail the preparation and characterisation of SWCNTs. Briefly, SWCNTs (CNI, Houston, TX) were produced by high pressure CO disproportionation (HiPco) method and purified by acid treatment to remove metal contaminants. Elemental analysis of the supplied SWCNTs by nitric acid dissolution and inductively coupled plasma-atomic emission spectrometry (ICP-AES, NMAM #7300) showed that the SWCNTs were 99% elemental carbon and 0.23% iron. The specific surface area was measured at -196°C by the nitrogen absorption–desorption technique (Brunauer Emmet Teller method) using an SA3100 Surface Area and Pore Size Analyzer (Beckman Coulter, Fullerton, CA). The diameter and length distribution of the SWCNTs were measured by field emission scanning electron microscopy. The surface area of the SWCNTs was 400–1000 m^2/g, and the width and length of individual SWCNT were 0.8–1.2 and 0.1–1 mm, respectively. SWCNTs were dispersed in culture media by Survanta®/sonication method as previously described (Wang et al. 2010a). Survanta is a natural lung surfactant that has been used in human clinical treatment and has been shown to be non-toxic to lung cells at the concentrations used in this study (Wang et al. 2010a). In all experiments, Survanta-containing medium was used as a control. The following table shows the final concentrations of SWCNT and Survanta used in various experiments.

Chemical and reagents

Antibodies against phospho-p38 MAPK and total p38 MAPK were obtained from Cell Signaling Technology, Inc. (Beverly, MA). Antibodies for collagen I and III were from Fitzgerald (Concord, MA). β-Actin antibody and horseradish peroxidase (HRP)-conjugated secondary antibodies were from Santa Cruz Biotechnology (Santa Cruz, CA). Human VEGF immunoassay kit, a neutralising antibody against VEGF and its non-specific control antibody, were from R&D Systems (Minneapolis, MN). LY−294002 (phosphoinositide 3-kinase (PI3K)/Akt inhibitor), PD98059 (extracellular-signal-regulated kinase (ERK)/MAPK inhibitor), SP600165 (c-Jun N-terminal Kinase (JNK) inhibitor), SB203580 (p38 MAPK inhibitor), CBO-P11 (VEGF inhibitor) and Mn (III) tetrakis (4-benzoic acid) porphyrin (MnTBAP) were obtained from Calbiochem (La Jolla, CA). Catalase (CAT) was from Roche Molecular Biochemicals (Indianapolis, IN). The oxidative probes, dichlorofluorescein diacetate (DCF-DA) and dihydroethidium (DHE) were from Molecular Probes (Eugene, OR). All other chemicals and reagents including *N*-acetyl cysteine (NAC) and LY364947 (TGF-β1 inhibitor) were from Sigma Chemical Inc. (St. Louis, MO).

Cell culture

The human lung fibroblasts CRL-1490 (ATCC; Manassas, VA) were maintained in Eagle's Minimum Essential

Survanta		SWCNT	
Stock (150 μg/ml)	Final concentration (μg/ml)	Stock (1 mg/ml)	Final concentration (μg/ml)
5 μl	0.75	5 μl	5
10 μl	1.5	10 μl	10
25 μl	3.75	25 μl	25

medium (MEM) supplemented with 10% foetal bovine serum (FBS), 100 U/ml penicillin and 100 μg/ml streptomycin. Human umbilical vein endothelial cells (HUVECs) were cultured in MCDB131 media (Gibco) supplemented with 25% FBS, 0.05% brain bovine extract, 0.25% endothelial cell growth supplement, 0.1% heparin, 1% L-glutamine and 0.1% gentamicin sulphate. HUVECs between passages two and five were used. Both the cell lines were cultured at 37°C in 5% CO_2 incubator and were passaged at preconfluent densities using a solution containing 0.05% trypsin and 0.5 mM EDTA.

Cell proliferation assay

Cells were plated in 96-well plates at a density of 1×10^3 cells/well in growth medium and were incubated for various time points. After specific treatments, the incubating medium was changed with 50 μl of 1X CyQUANT™ dye-binding solution (Invitrogen) and incubated for 60 min at 37°C. The fluorescence intensity of each sample was measured at the excitation and emission wavelengths of 485 and 535 nm, respectively.

Collagen assays

Collagen expression was determined by western blotting and cellular collagen content was determined by Sircol® assay (Biocolor Ltd., Belfast, UK), according to the manufacturer's protocol. Briefly, Sirius red reagent (50 μl) was added to cell culture supernatant (50 μl) and mixed for 30 min. The collagen–dye complex was precipitated by centrifugation at 13,000 g for 5 min, washed with ethanol and dissolved in 0.5 M NaOH. The samples were read for absorbance at 540 nm.

Western blot analysis

After specific treatments, cells were harvested and lysed on ice for 30 min in lysis buffer containing 150 mM NaCl, 100 mM Tris (pH 8.0), 1% Triton X-100, 1% deoxycholic acid, 0.1% SDS, 5 mM EDTA, 10 mM sodium formate, 1 mM sodium orthovanadate, 2 mM leupeptin, 2 mM aprotinin, 1 mM phenylmethylsulphonyl fluoride, 1 mM dithiothreitol and 2 mM pepstatin A. After centrifugation at 14,000 g for 15 min at 4°C, the supernatant was collected as the total cellular protein extract. The protein concentrations were determined using a bicinchoninic acid protein assay kit (Pierce Biotechnology, Rockford, IL). Equal amount of proteins per sample (20 μg) were resolved on a 10% sodium dodecyl sulphate-polyacrylamide gel electrophoresis (SDS-PAGE) and transferred onto a nitrocellulose membrane. The membrane was blocked with T-PBS (0.3% Tween-20 in PBS) containing 5% dry milk and incubated with primary antibody overnight at 4°C. After three washes with T-PBS, the membrane was incubated with HRP-conjugated secondary antibody for 1 h and then washed with 0.05% Tween-20 in PBS. Immunoreactive proteins were detected by chemiluminescence (Supersignal® West Pico, Pierce, Rockford, IL) and quantified by imaging densitometry using UN-SCAN-IT digitising software (Silk Scientific, Orem, UT). Mean densitometry data from independent experiments were normalised to results in cells from control experiments.

ROS detection

Cellular ROS production was determined fluorometrically using DHE and DCF-DA as fluorescent probes for superoxide and peroxide, respectively. After specific treatments, cells were incubated with the probes (10 μM) for 30 min at 37°C, after which they were washed, resuspended in PBS and analysed for fluorescence intensity using a multi-well plate reader (FLUOstar OPTIMA, BMG LABTECH Inc., Durham, NC) at the excitation/emission wavelengths of 485/535 and 485/610 nm for DHE and DCF fluorescence measurements, respectively.

Enzyme-linked Immunosorbent Assays (ELISAs)

Cells were plated in a six-well plate at a density of 2×10^5 cells/well in culture medium and incubated overnight before the cells were subjected to treatment. After the treatment, cell supernatants were collected and analysed for either TGF-β1 or VEGF protein levels using a respective Quantikine ELISA kits (R&D Systems, Minneapolis, MN) as per the manufacturer's protocol. Briefly, cell samples or reference standards (100 μl) were added to the wells of a microplate that was pre-coated with a monoclonal antibody specific to either TGF-β1 or VEGF and incubated for 2 h at room temperature. After washing unbounded substances, an HRP-conjugated polyclonal antibody against either TGF-β1 or VEGF was added to the wells and incubated for 2 h at room temperature. After washing and adding 100 μl of substrate solution, optical density was determined on a microplate reader at 450 nm.

Angiogenesis tube formation assay

Growth factor-reduced Matrigel® (Becton Dickinson) was placed in 24-well plates (150 μl/well) and allowed to set at 37°C for 30 min. HUVECs (5×10^4) suspended in 2.5% dialysed FBS medium containing the specific treatments were added to each well and incubated at 37°C for 24 h. The morphological changes were observed and photographed using phase contrast microscope (5X). Each well was photographed and the number of nodes formed was scored manually from at least five different fields for each well.

Statistical analysis

The data represent mean ± SD from three or more independent experiments. Statistical analysis was performed by analysis of variance and Duncan's comparison tests were used to evaluate the significance between measurements at a significance level of $p < 0.05$.

Results

SWCNTs induce fibroblast proliferation and collagen production

To determine the effect of SWCNTs on fibroblast proliferation and collagen production, human lung fibroblast CRL-1490 cells were treated with various concentrations of SWCNTs and analysed for cell growth by CyQUANT™ cell proliferation assay. Figure 1A and B show that SWCNTs induced fibroblast proliferation in a dose- and

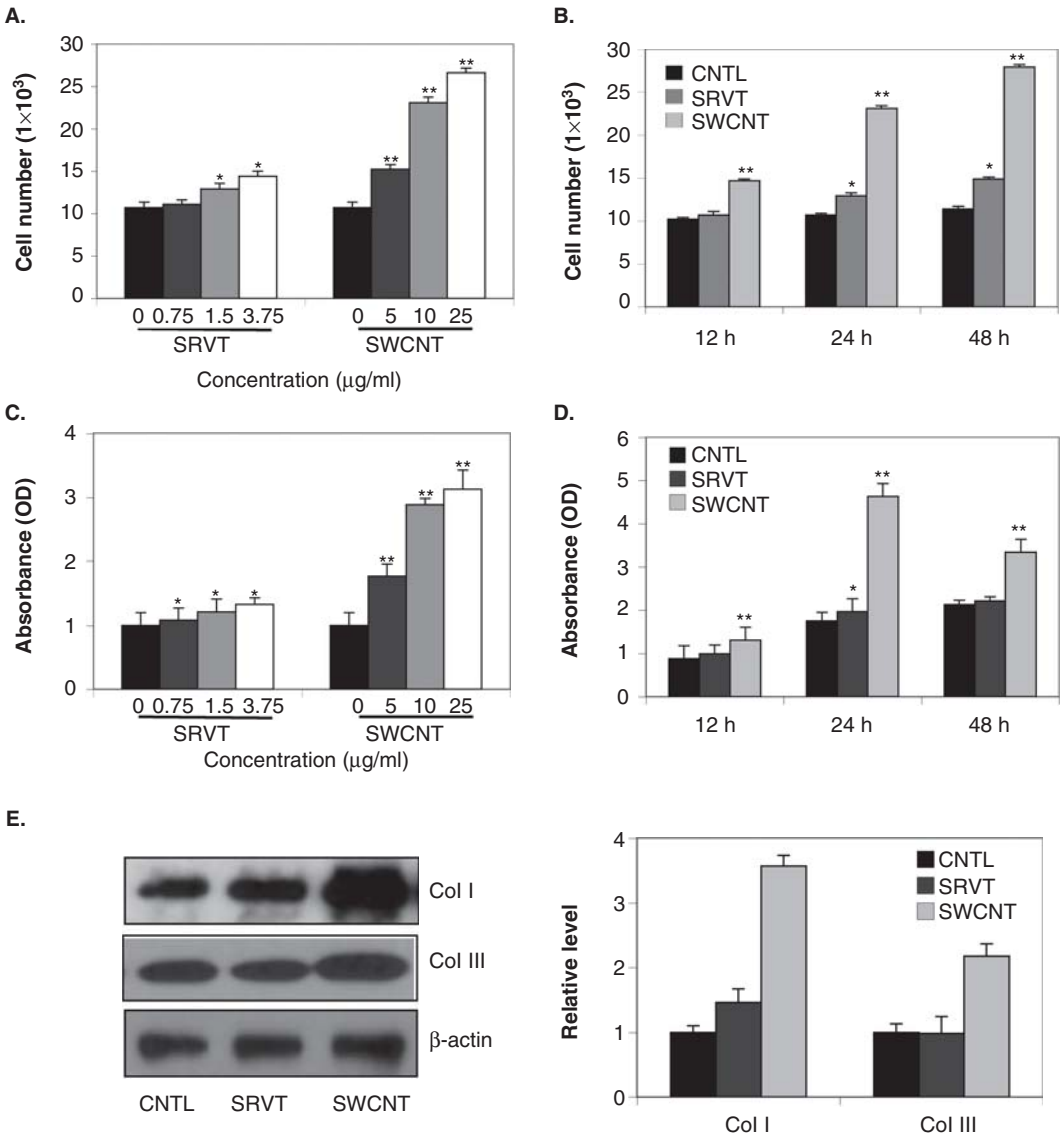

Figure 1. Single-walled carbon nanotube (SWCNT)-induced fibroblast proliferation and collagen expression. A. Subconfluent cultures of human lung fibroblast CRL-1490 cells were exposed to various concentrations of vehicle control Survanta (SRVT) (0–3.75 μg/ml) or SWCNTs (0–25 μg/ml) and analysed for cell growth after 24 h by CyQUANT™ cell proliferation assay. B. CRL-1490 cells were exposed to SRVT (1.5 μg/ml) and SWCNTs (10 μg/ml) and analysed for cell growth at various times (0–48 h). C. Subconfluent cultures of CRL-1490 cells were exposed to various concentrations of SRVT (0–3.75 μg/ml) and SWCNTs (0–25 μg/ml) for 24 h. Cell supernatants were collected and analysed for soluble collagen content by Sircol® collagen assay. D. CRL-1490 cells were exposed to SRVT (1.5 μg/ml) and SWCNTs (10 μg/ml) and analysed for soluble collagen content by Sircol® collagen assay at various times (0–48 h). E. Cells treated with SRVT (1.5 μg/ml) and SWCNTs (10 μg/ml) for 24 h were analysed for human collagen type I and III by western blotting. Blots were reprobed with β-actin antibody to confirm equal loading of the samples. The immunoblot signals were quantified by densitometry. Mean densitometry data from independent experiments (one of which is shown here) were normalised to the result obtained in cells in the absence of SRVT and SWCNTs (nontreated control). Plots are mean ± SD ($n = 4$). *, $p < 0.05$ *versus* nontreated control. **, $p < 0.05$ *versus* nontreated control and corresponding SRVT treatment.

time-dependent manner. Analysis of total collagen content in SWCNT-treated cell supernatant by Sircol® collagen assay showed a similar time- and dose-dependent effect on soluble collagen content (Figure 1C and D). Vehicle control (Survanta)-treated cells showed minimal response. Induction of two of the most abundant collagen proteins of the ECM, viz., collagen I and III (Brinckerhoff and Matrisian 2002; Pardo & Selman 2005), was also measured in response to SWCNTs and Survanta exposure (Figure 1E). SWCNTs strongly induced collagen I and III levels. The induction of collagen by SWCNTs was independent of its effect on cell growth since collagen expression was determined on the basis of equal cellular protein per sample. Together, these results indicate that SWCNTs was able to directly induce fibrogenic effects such as fibroblast proliferation and collagen production in CRL-1490 cells.

Involvement of ROS in SWCNTs-induced fibrogenesis

Since increased ROS production is tightly linked with pulmonary fibrosis (Inghilleri et al. 2006; Quinlan et al. 1994), we investigated the effect of SWCNTs on cellular ROS. Survanta was used as a control. SWCNTs induce a dose-dependent increase in cellular DCF fluorescence intensities, indicative of peroxide formation, but had minimal effect on DHE fluorescence indicative of superoxide formation (Figure 2A and B). To determine the role of ROS

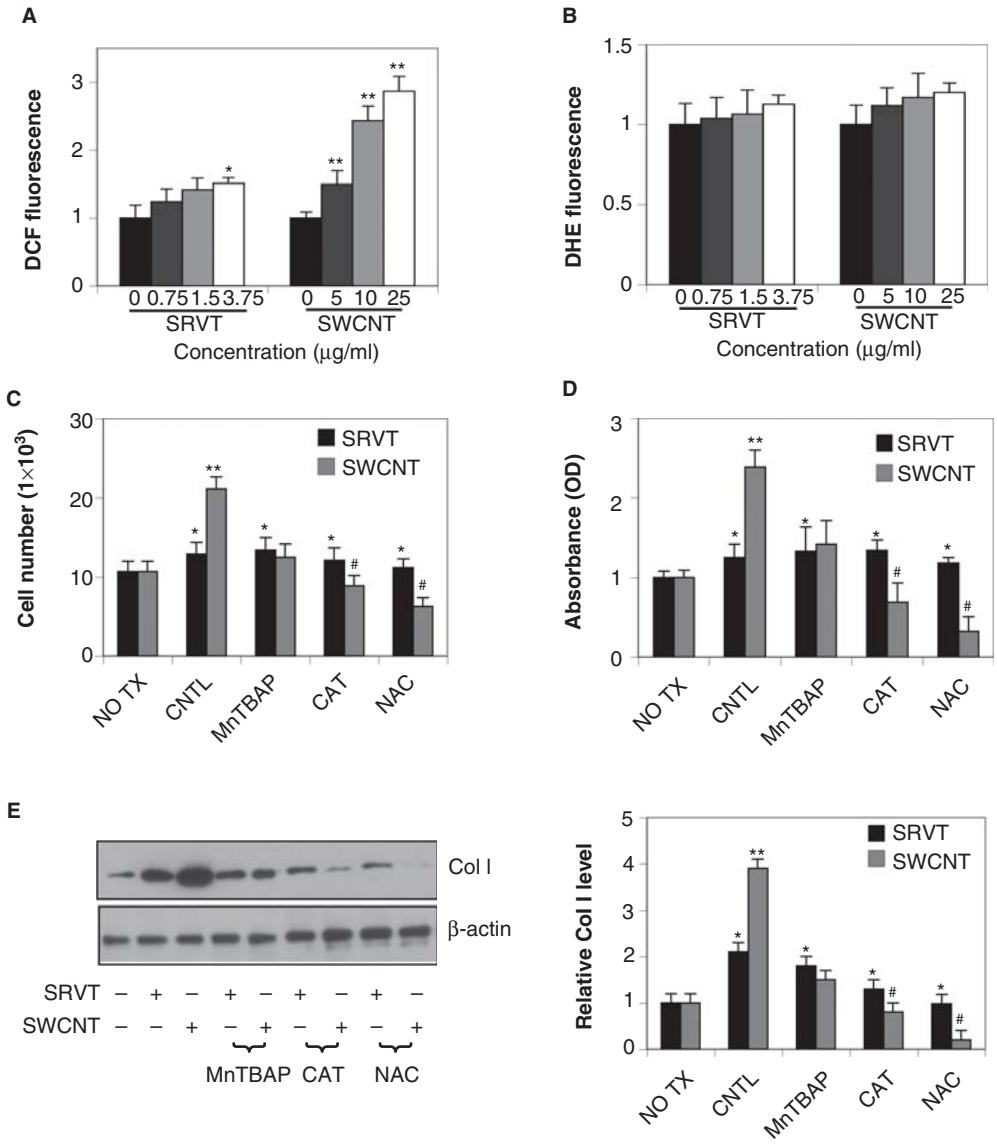

Figure 2. Involvement of reactive oxygen species (ROS) on single-walled carbon nanotube (SWCNT)-induced collagen expression and fibroblast proliferation. A and B. CRL-1490 cells were treated with various concentrations of Survanta (SRVT) (0–3.75 μg/ml) and SWCNTs (0–25 μg/ml) and analysed for ROS production by measuring DCF and DHE fluorescence intensities. Plots show relative fluorescence intensity over nontreated control at the peak response time of 3 h after the treatment. C. CRL-1490 cells were pretreated for 1 h with NAC (10 mM), MnTBAP (100 μM) or catalase (CAT) (1000 U/ml), and then treated with SRVT (150 μg/ml) or SWCNTs (10 μg/ml) for 24 h and analysed for cell growth. D. CRL-1490 cells were pretreated for 1 h with NAC (10 mM), MnTBAP (100 μM) or CAT (1,000 U/ml) and then treated with SRVT (1.5 μg/ml) and SWCNTs (10 μg/ml). Cell supernatants were analysed for soluble collagen content by Sircol® collagen assay after 24 h. E. Cells were pretreated for 1 h with NAC (10 mM), MnTBAP (100 μM) or CAT (1000 U/ml) and then treated with SRVT (1.5 μg/ml) and SWCNTs (10 μg/ml) for 24 h and analysed for collagen I by western blotting. Blots were reprobed with β-actin antibody to confirm equal loading of the samples. The immunoblot signals were quantified by densitometry. Plots are mean ± SD ($n = 4$). *, $p < 0.05$ *versus* nontreated control. **, $p < 0.05$ *versus* nontreated control and corresponding SRVT treatment. #, $p < 0.05$ *versus* SWCNT control and corresponding SRVT treatment.

on SWCNT-induced fibrogenic effects, cells were treated with SWCNTs in the presence or absence of various ROS inhibitors including MnTBAP (superoxide scavenger), catalase (hydrogen peroxide scavenger) and NAC (general antioxidant). MnTBAP, catalase and NAC inhibited the proliferative and collagen-inducing effects of SWCNTs (Figure 2C–E). SWCNTs did not significantly induce superoxide production, and although MnTBAP inhibited SWCNT-induced fibrogenic effects, catalase showed a dominant effect. Together, these results support the role of ROS, particularly peroxides, as a key regulator of SWCNT-induced fibrogenesis.

SWCNT-induced fibrogenic effects are mediated through p38 MAPK pathway

To determine the major cell survival pathway involved in SWCNT-induced fibrosis, cells were treated with SWCNTs and inhibitors of various cell survival pathways including LY294002 (PI3K/Akt inhibitor), SP200165 (JNK inhibitor), SB203580 (p38 MAPK inhibitors) and PD98059 (ERK/MAPK inhibitor), and their effects on fibroblast proliferation and collagen expression were determined (Figure 3A and B). SB203580 significantly inhibited SWCNT-induced fibroblast proliferation and collagen expression whereas all the other inhibitors had minimal effect. Furthermore, SWCNTs were

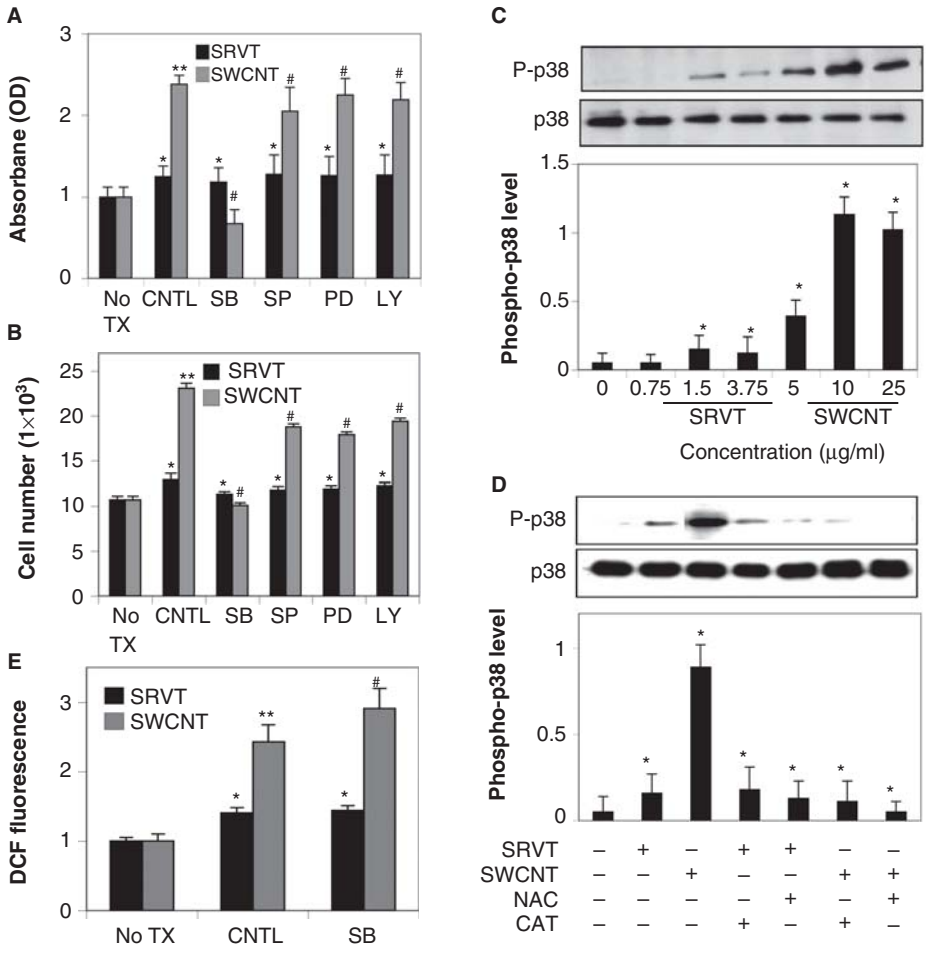

Figure 3. Single-walled carbon nanotube (SWCNT)-induced fibrogenic effects are mediated through p38 mitogen-activated protein kinase (MAPK) pathway. A. CRL-1490 cells were pretreated for 1 h with LY294002 (10 μM), SP200165 (10 μM), SB203580 (10 μM) and PD98059 (10 μM) and then treated with Survanta (SRVT) (1.5 μg/ml) or SWCNTs (10 μg/ml). Cell supernatants were analysed for soluble collagen content by Sircol® collagen assay after 24 h. B. CRL-1490 cells were pretreated for 1 h with LY294002 (10 μM), SP200165 (10 μM), SB203580 (10 μM) or PD98059 (10 μM) and then treated with SRVT (150 μg/ml) or SWCNTs (10 μg/ml) for 24 h and analysed for cell growth. C. CRL-1490 cells were treated with various concentrations of SRVT (0–3.75 μg/ml) and SWCNTs (0–25 μg/ml) for 6 h after which they were washed with PBS and extracted with SDS sample buffer. The cell extracts were separated on 10% polyacrylamide-SDS gels, transferred and probed with antibodies against phospho-p38 MAPK and total p38 MAPK. The immunoblot signals were quantified by densitometry. D. Cells were either left untreated or pretreated with NAC (10 mM) or catalase (CAT) (1000 U/ml) for 1 h, followed by SRVT (1.5 μg/ml) or SWCNTs (10 μg/ml) for 6 h. Cell lysates were prepared and analysed for phospho-p38 MAPK and total p38 MAPK. The immunoblot signals were quantified by densitometry. E. CRL-1490 cells were pretreated for 1 h with SB203580 (10 μM) and then treated with SRVT (1.5 μg/ml) or SWCNTs (10 μg/ml) for 3 h. Samples were analysed for reactive oxygen species (ROS) production by measuring DCF fluorescence intensity. Plots are mean ± SD ($n = 3$). *, $p < 0.05$ *versus* nontreated control. **, $p < 0.05$ *versus* nontreated control and corresponding SRVT treatment. #, $p < 0.05$ *versus* SWCNT control and corresponding SRVT treatment.

able to induce p38 phosphorylation in a dose- and time-dependent manner, whereas it had no significant effect on total p38 protein level (Figure 3C). SWCNTs had minimal effect on all the other cell survival pathways (data not shown). Additionally, ROS inhibitors significantly inhibited SWCNT-induced p38 phosphorylation indicating that SWCNT-mediated ROS generation is required for p38 MAPK activation (Figure 3D). Interestingly, treatment with specific p38 MAPK inhibitor SB203580 significantly increased cellular peroxide levels indicating that there is a negative feedback loop between ROS and p38 MAPK in response to SWCNT exposure (Figure 3E).

SWCNT-mediated TGF-β1 activation via the p38 MAPK pathway

TGF-β1 is one of the key regulators of lung fibrosis, and increased expression of TGF-β1 has been consistently reported in biopsies of fibrotic lungs (Coker et al. 1997; McAnulty & Laurent 1995; Papakonstantinou et al. 2003; Pelton et al. 1989). SWCNTs induced a dose-dependent increase in TGF-β1 activation as assessed by human TGF-β1 ELISA (Figure 4A). ROS inhibitors (catalase and NAC) and p38 MAPK inhibitor (SB203580) significantly inhibited SWCNT-induced TGF-β1 activation (Figure 4B). TGF-β1 and TGF-β1 inhibitor (LY364947) were used as positive and negative controls. These modulators had no significant effect either on ROS production or on p38 MAPK activation, indicating that SWCNT-induced TGF-β1 activation is downstream of p38 MAPK pathway and is being regulated by SWCNT-induced ROS production (Figure 4C and D). Furthermore, TGF-β1 played a significant role in SWCNT-induced fibrogenic effects. Pretreatment of cells with TGF-β1 increased SWCNT-induced collagen production and fibroblast cell proliferation, whereas TGF-β1

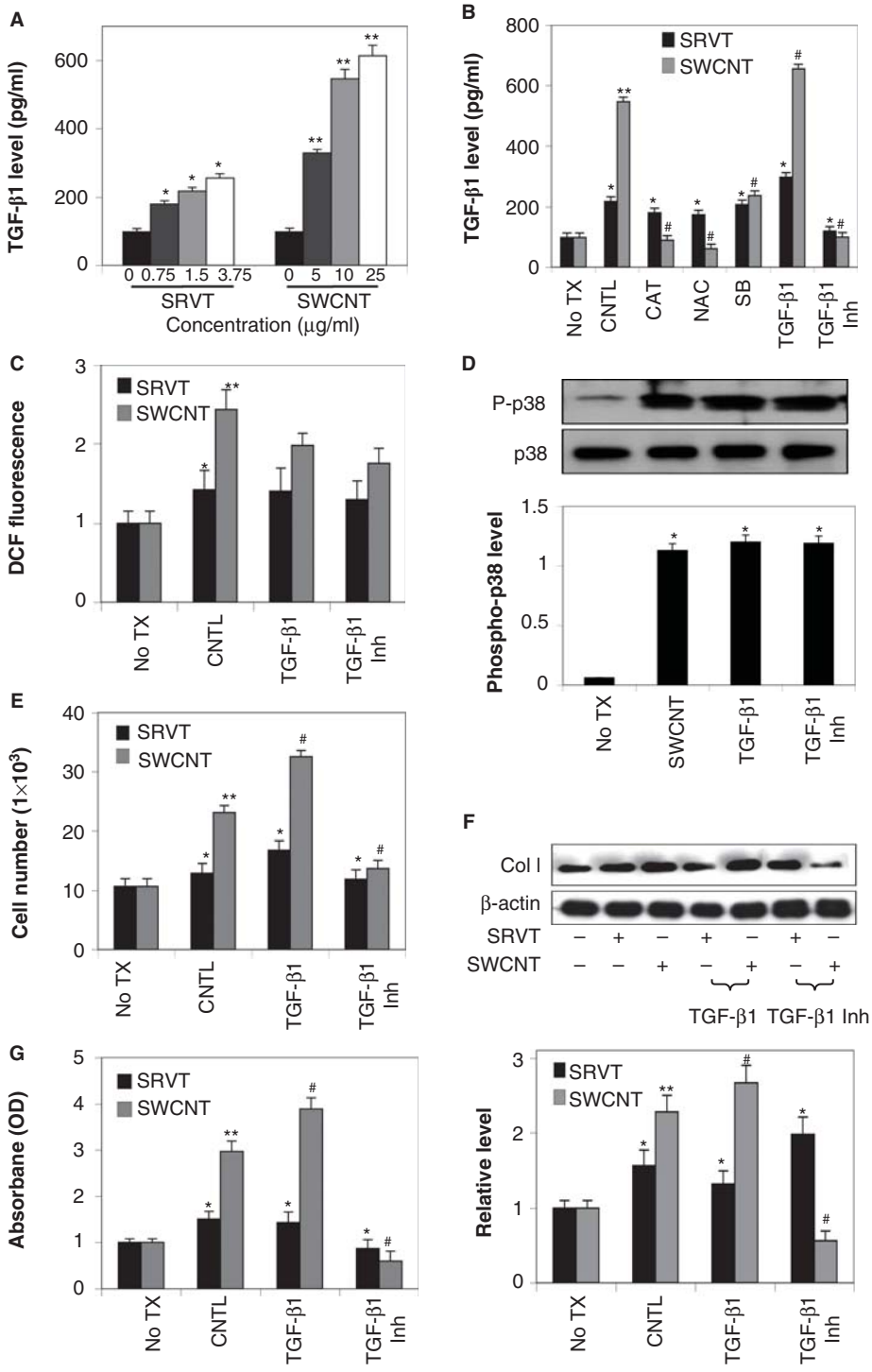

Figure 4. Single-walled carbon nanotube (SWCNT)-induced TGF-β1 activation through reactive oxygen species (ROS)-mediated p38 mitogen-activated protein kinase (MAPK) pathway. A. CRL-1490 cells were treated with various concentrations of Survanta (SRVT) (0–3.75 μg/ml) and SWCNTs (0–25 μg/ml) for 24 h and analysed for TGF-β1 by ELISA. B. Cells were pretreated for 1 h with NAC (10 mM), catalase (CAT) (1000 U/ml), SB203580 (10 μM), TGF-β1 (100 ng/ml) or TGF-β1 inhibitor (LY364947) (10 μM) and then treated with SRVT (1.5 μg/ml) and SWCNTs (10 μg/ml) for 24 h and analysed for TGF-β1 by ELISA. C. CRL-1490 cells were pretreated for 0.5 h with TGF-β1 (100 ng/ml) or TGF-β1 inhibitor (10 μM) and then treated with SRVT (1.5 μg/ml) and SWCNTs (10 μg/ml) for 3 h. Samples were analysed for ROS production by measuring DCF fluorescence intensity. Plots show relative fluorescence intensity over nontreated control at the peak response time of 3 h after the treatment. D. Cells were either left untreated or pretreated with TGF-β1 (100 ng/ml) or TGF-β1 inhibitor (LY364947) (10 μM) for 1 h, followed by SWCNTs (10 μg/ml) for 6 h. Cell lysates were prepared and analysed for phospho-p38 MAPK and total p38 MAPK. The immunoblot signals were quantified by densitometry. E. CRL-1490 cells were pretreated for 1 h with TGF-β1 (100 ng/ml) or TGF-β1 inhibitor (LY364947) (10 μM) and then treated with SRVT (1.5 μg/ml) or SWCNTs (10 μg/ml) for 24 h and analysed for cell growth. F. CRL-1490 cells were pretreated for 1 h with TGF-β1 (100 ng/ml) or TGF-β1 inhibitor (10 μM) and then treated with SRVT (1.5 μg/ml) and SWCNTs (10 μg/ml). Cell supernatants were analysed for soluble collagen content by Sircol® collagen assay after 24 h. G. Cells were pretreated for 1 h with TGF-β1 (100 ng/ml) or TGF-β1 inhibitor (10 μM) and then treated with SRVT (1.5 μg/ml) and SWCNTs (10 μg/ml) for 24 h and analysed for collagen I by western blotting. Blots were reprobed with β-actin antibody to confirm equal loading of the samples. The immunoblot signals were quantified by densitometry. Plots are mean ± SD ($n = 4$). *, $p < 0.05$ *versus* nontreated control. **, $p < 0.05$ *versus* nontreated control and corresponding SRVT treatment. #, $p < 0.05$ *versus* SWCNT control and corresponding SRVT treatment.

inhibitor (LY364947) showed a significant decrease in SWCNT-induced fibrogenic effects (Figure 4E–G).

SWCNT-induced VEGF plays a key role in fibrogenesis

VEGF is a known target of p38 MAPK signalling (Demyanets et al. 2011; Hiratsuka et al. 2011; Shields et al. 2011) and is upregulated in fibrotic lungs (Fehrenbach et al. 1999; Meyer et al. 2000; Steurer et al. 2007). Since p38 MAPK was activated by SWCNTs, we tested the effect of SWCNTs on VEGF level. Cells were treated with SWCNTs and cell supernatant were collected and analysed for VEGF at various times by ELISA. Figure 5A shows that VEGF protein levels were induced by the SWCNTs treatment in a dose-dependent manner. The induction of VEGF by SWCNTs was significantly inhibited by NAC, catalase and p38 MAPK inhibitor SB203580 (Figure 5B), indicating that SWCNT-induced VEGF production may be through the p38 MAPK pathway via ROS generation. Similar to TGF-β 1, VEGF showed no significant effect on SWCNT-mediated ROS generation and p38 MAPK activation (Figure 5C and D). Since VEGF was a key effecter molecule of the p38 MAPK pathway, we tested whether VEGF was a key mediator of SWCNT-induced fibrogenic effects. Cells were treated with VEGF and cell proliferation and collagen expression were determined. Figure 5E and F show that VEGF induced collagen expression and fibroblast proliferation. Interestingly, a positive feedback loop was observed between VEGF and TGF-β1. VEGF increased TGF-β1 levels whereas VEGF inhibitor significantly inhibited TGF-β1 levels (Figure 5G). TGF-β1 modulators showed a similar effect on VEGF activation (Figure 5H).

SWCNTs induce an angiogenic response

Since VEGF is the central regulator of angiogenesis and TGF-β1 is also known to be pro-angiogenic, we analysed the capability of SWCNTs to induce angiogenesis. HUVECs were treated with various concentrations of SWCNTs and analysed for angiogenesis by *in vitro* tube formation assay. SWCNTs induced angiogenesis in a dose-dependent manner (Figure 6A). To correlate the response to SWCNT-induced fibrogenesis, CRL-1490 fibroblasts were treated with varying concentrations of SWCNTs or Survanta, and cell supernatant were collected and used to induce angiogenesis in HUVECs (Figure 6B). The induction of angiogenesis was more pronounced with SWCNT-treated fibroblast supernatant as compared with direct SWCNT treatment. We next treated lung fibroblasts with modulators of ROS, p38 MAPK, TGF-β1 and VEGF along with SWCNTs. Cell supernatants were collected and used to induce angiogenesis in HUVECs (Figure 6C). ROS, p38 MAPK, TGF-β1 and VEGF inhibitors significantly inhibited SWCNT-induced angiogenesis whereas TGF-β1 and VEGF treatments further increased SWCNT-induced angiogenesis. HUVECs treated directly with various modulators of ROS, p38 MAPK, TGF-β1 and VEGF showed similar effect on SWCNT-induced angiogenesis (data not shown). The effect was more pronounced with treated fibroblast supernatants as compared with direct treatments. The results indicated that SWCNT-induced fibrogenic mediators played a key role in SWCNT-induced angiogenic response.

Discussion

Pulmonary cytotoxicity and associated fibrosis in response to SWCNT exposure are well documented (Wang et al. 2010b). In this study, we investigated the role of ROS and specific signalling pathways in fibrogenesis and angiogenesis induced by SWCNTs. Several mechanisms of pulmonary fibrosis have been proposed, including epithelial cell injury, basement membrane disruption, ECM remodelling and angiogenesis. Following injury, the epithelium initiates a wound-healing process to restore the integrity of its barrier. This is facilitated by connective tissue cells, in particular fibroblasts that produce ECM that promotes epithelial cell migration and re-epithelialisation (Selman et al. 2001). Uncontrolled or excessive production of ECM by fibroblasts is believed to be a key contributing factor in the development of lung fibrosis. In our study, SWCNT exposure led to increased fibroblast proliferation and collagen production (Figure 1). Activation of fibroblast proliferation and accumulation of ECM during the repair process necessitates neovascularisation, and increasing evidence support its role in fibrosis (Brinckerhoff & Matrisian 2002; Selman et al. 2001; Selman et al. 1986). The angiogenic process is known to involve an intricate cytokine network that activates and mediates interactions between multiple cell types. A key mediator of angiogenesis is VEGF, which is overexpressed in fibrotic lungs (Carmeliet 2000; Steurer et al. 2007). In this study, we demonstrate for the first time that SWCNT exposure increased VEGF protein levels and induced an angiogenic response in vascular endothelial cells (Figures 5A and 6A).

ROS plays a key role in various cellular processes, but its regulatory role in fibrosis and angiogenesis are unclear. SWCNT-induced ROS played significant role in SWCNT-induced fibrogenic effects (Figure 2C and D). SWCNTs induced significant levels of peroxides, but its effect on superoxide was minimal (Figure 2A and B). Furthermore, superoxide scavenger MnTBAP blocked SWCNT-induced fibrogenic effects but catalase (hydrogen peroxide inhibitor) showed a more dominant effect. Interestingly, various ROS inhibitors significantly blocked SWCNT-induced angiogenesis revealing an additional unexplored avenue in SWCNTs toxicity that could be potentially targeted (Figure 6C). The role of various signal transduction pathways in cell survival and angiogenesis is well established but their role in fibrogenesis is unclear. In response to SWCNTs exposure, p38 MAPK cell survival pathway played a key role in its fibrogenic and angiogenic responses. SWCNTs induced phosphorylation and activation of p38 MAPK required ROS generation (Figure 3). ROS inhibitors, NAC and catalase inhibited SWCNT-induced phosphorylation and activation of p38 MAPK (Figure 3D), supporting the role of p38 MAPK and its regulation by ROS in the fibrogenic process. The requirement of ROS in SWCNT-induced p38 MAPK activation and fibrogenesis has not been reported, and our results provide new evidence thus revealing a novel mechanism of fibrogenesis regulation that could have important implications in anti-fibrotic therapy. Interestingly, treatment with SB203580 increased cellular peroxide levels (Figure 3E)

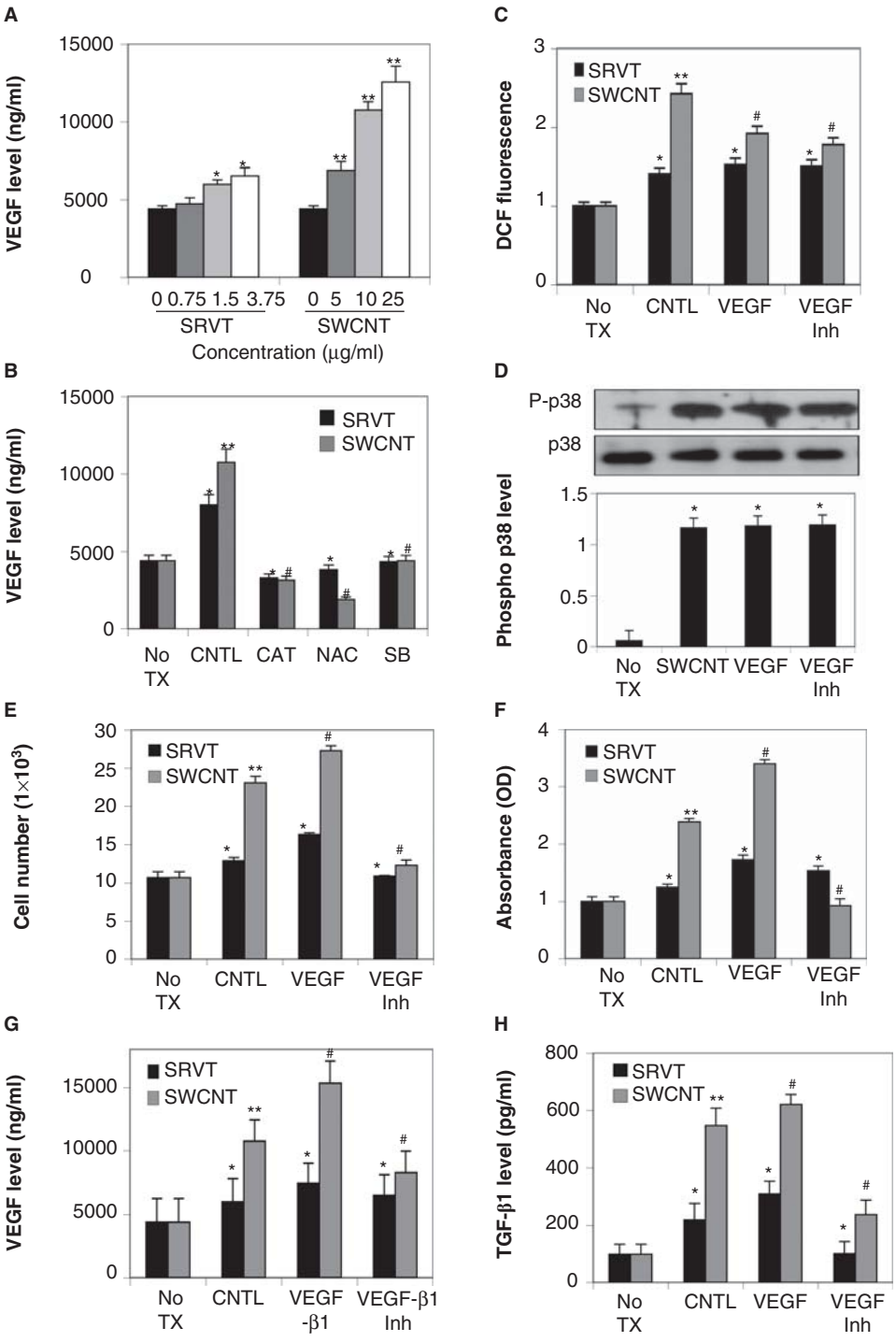

Figure 5. Single-walled carbon nanotube (SWCNT)-induced VEGF plays a key role in fibrogenesis. A. CRL-1490 cells were treated with various concentrations of Survanta (SRVT) (0–3.75 μg/ml) and SWCNTs (0–25 μg/ml) for 24 h and analysed for VEGF by ELISA. B. CRL-1490 cells were either left untreated or pretreated with NAC (10 mM), catalase (CAT) (1000 U/ml) or SB203580 (10 μM) for 1 h and then treated with SRVT (1.5 μg/ml) or SWCNTs (10 μg/ml) for 24 h. Samples were analysed for VEGF by ELISA. C. CRL-1490 cells were pretreated for 0.5 h with VEGF (100 nm) or VEGF inhibitor (CBO-P11) (10 μm) and then treated with SRVT (1.5 μg/ml) or SWCNTs (10 μg/ml) for 3 h. Samples were analysed for reactive oxygen species (ROS) production by measuring DCF fluorescence intensity. Plots show relative fluorescence intensity over nontreated control at the peak response time of 3 h after the treatment. D. Cells were either left untreated or pretreated with VEGF (100 nm) or VEGF inhibitor (CBO-P11) (10 μm) for 1 h, followed by SWCNTs (10 μg/ml) for 6 h. Cell lysates were prepared and analysed for phospho-p38 mitogen-activated protein kinase (MAPK) and total p38 MAPK. The immunoblot signals were quantified by densitometry. E. CRL-1490 cells were pretreated for 1 h with VEGF (100 nm) or VEGF inhibitor (CBO-P11) (10 μm) and then treated with SRVT (1.5 μg/ml) or SWCNTs (10 μg/ml) for 24 h and analysed for cell growth. F. CRL-1490 cells were pretreated for 1 h with VEGF (100 nm) or VEGF inhibitor (10 μm) and then treated with SRVT (1.5 μg/ml) or SWCNTs (10 μg/ml) for 24 h. Cell supernatants were analysed for soluble collagen content by Sircol® collagen assay. G. Cells were either left untreated or were pretreated with TGF-β1 (100 ng/ml) and TGF-β1 inhibitor (LY364947) (10 μM) followed by SRVT (1.5 μg/ml) or SWCNTs (10 μg/ml) for 24 h. Samples were analysed for VEGF by ELISA. H. CRL-1490 cells were pretreated for 1 h with VEGF (100 nm) or VEGF inhibitor (10 μm) and then treated with SRVT (1.5 μg/ml) or SWCNTs (10 μg/ml) for 24 h and analysed for TGF-β1 by ELISA. Plots are mean ± SD ($n = 3$). *, $p < 0.05$ *versus* nontreated control, **, $p < 0.05$ *versus* nontreated control and corresponding SRVT treatment. #, $p < 0.05$ *versus* SWCNT control and corresponding SRVT treatment.

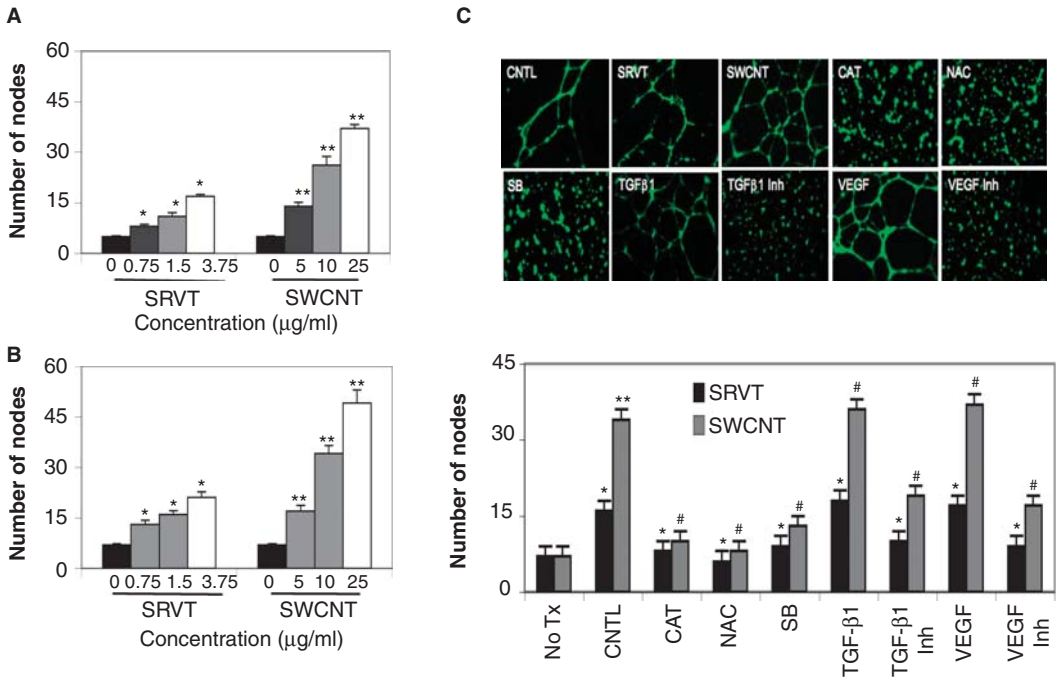

Figure 6. Single-walled carbon nanotubes (SWCNTs) induce an angiogenic response. A. Human umbilical vein endothelial cells (HUVECs) were treated with various concentrations of Survanta (SRVT) (0–3.75 μg/ml) and SWCNTs (0–25 μg/ml) for 48 h and analysed for angiogenesis by tube formation assay. The number of nodes formed by the tubes were scored and plotted. B. CRL-1490 cells were treated with various concentrations of SRVT (0–3.75 μg/ml) and SWCNTs (0–25 μg/ml) for 24 h and cell culture supernatant were used to induce angiogenesis in HUVECs for 48 h and were analysed by *in vitro* tube formation assay. Representative micrographs after staining with calcein-AM. C. CRL-1490 cells were either left untreated or pretreated with NAC (10 mM), catalase (CAT) (1000 U/ml), SB203580 (10 μM), TGF-β1 (100 ng/ml), TGF-β1 inhibitor (LY364947) (10 μM), VEGF (100 nm) or VEGF inhibitor (CBO-P11) (10 μm) for 1 h and then treated with SRVT (1.5 μg/ml) or SWCNTs (10 μg/ml) for 24 h. Cell culture supernatant were used to induce angiogenesis in HUVECs for 48 h and were analysed by *in vitro* tube formation assay. Representative micrographs after staining with calcein-AM. Plots are mean ± SD ($n = 3$). *, $p < 0.05$ *versus* nontreated control, **, $p < 0.05$ *versus* nontreated control and corresponding SRVT treatment. #, $p < 0.05$ *versus* SWCNT control and corresponding SRVT treatment.

indicative of a negative feedback loop between p38 MAPK and ROS. This may suggest that downregulation of p38 MAPK levels triggers a feedback mechanism leading to increased ROS production, which leads to reactivation of p38 MAPK and may possibly exacerbate fibrogenic and angiogenic effects in response to SWCNTs.

SWCNT-induced VEGF and angiogenic response was inhibited by the p38 MAPK inhibitor SB203580 (Figures 5B and 6C). Therefore, in response to SWCNTs, p38 MAPK may be the major signalling pathway regulating VEGF and angiogenesis. Since ROS regulates p38 MAPK signalling in response to SWCNTs treatment, it is likely that ROS may serve as an upstream regulator of the fibrogenic signalling via p38 MAPK–VEGF pathway. VEGF was induced by SWCNTs (Figure 5A) and its neutralisation by anti-VEGF antibody significantly inhibited the fibrogenic effects of SWCNTs (Figure 5E and F). However, such inhibition was incomplete, and increasing the concentration of the neutralising antibody beyond the indicated concentration did not result in further inhibition indicating that VEGF alone could not account for the total fibrogenic effects of SWCNTs. These results suggest that although VEGF could be a key mediator of the fibrogenic effect of SWCNTs, other mediators or other mechanisms of fibroblast activation are also involved. Several growth factors under the regulation of p38 MAPK including platelet-derived growth factor (PDGF) and TGF-β1 have been reported (Huh et al. 2011; Kolosova et al. 2011; Roos et al. 2011). These growth factors along with several others including basic fibroblast growth factor and VEGF have also been reported to regulate p38 MAPK (Goldberg et al. 2002; Sorensen et al. 2008; Xiong et al. 2001; Zhang et al. 2011). In response to SWCNTs, p38 MAPK regulated TGF-β1 levels whereas TGF-β1 had no significant effect on phosphorylation and activation of p38 MAPK. Interestingly, increased expression of TGF-β1 has been consistently reported in biopsies of fibrotic lungs as well as in angiogenically active tissues (Roberts et al. 1986). We observed that TGF-β1 plays a critical role in response to SWCNTs, regulating not only SWCNT-mediated fibrogenic but also angiogenic effects. TGF-β1 significantly increased SWCNT-mediated cell proliferation and collagen expression whereas TGF-β1 inhibitor (LY364947) showed opposite effects (Figure 4E–G). Furthermore, TGF-β1 inhibitor significantly inhibited SWCNT-induced angiogenesis and TGF-β1 further increased the effect (Figure 6C). TGF-β1 had no significant effect on ROS levels but ROS scavengers significantly inhibited TGF-β1 levels, indicating that SWCNT-induced ROS regulated TGF-β1 activation (Figure 4B and C). Interestingly, TGF-β1 inhibitor inhibited VEGF levels and VEGF inhibitor also inhibited TGF-β1 levels, indicating a positive autocrine loop between VEGF and TGF-β1 (Figure 5G and H). This is an interesting novel finding, as both VEGF and TGF-β1 are pro-angiogenic and pro-fibrotic. A positive autocrine loop between the two biomolecules may

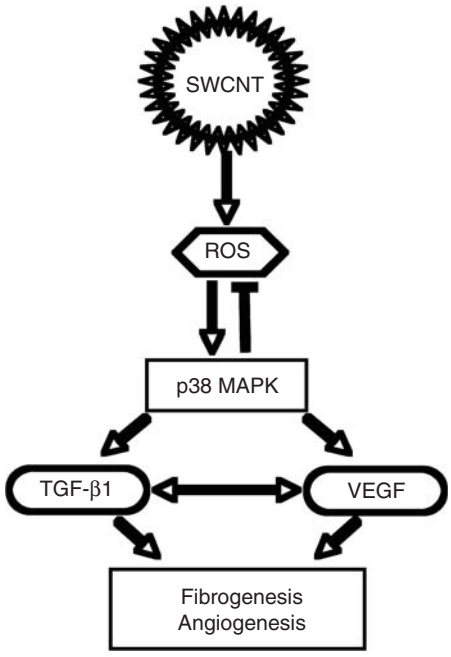

Figure 7. Schematic representation of mechanisms involved in single-walled carbon nanotube (SWCNT)-induced fibrogenesis and angiogenesis.

produce an additive effect further exacerbating SWCNT-induced pathogenesis.

Conclusions

In summary, this study provides evidence that in addition to the fibrogenic effects, SWCNTs are capable of inducing an angiogenic response. SWCNTs induce a direct fibrogenic effect on lung fibroblasts by upregulating collagen expression and cell proliferation through ROS generation. The p38 MAPK pathway regulated SWCNT-induced fibrogenesis through multiple mechanisms involving various cytokines and growth factors including TGF-β1 and VEGF. Both TGF-β1 and VEGF significantly contributed to the fibrogenic as well as angiogenic effect of SWCNTs. Figure 7 is a schematic representation of the mechanisms involved in response to SWCNT exposure. SWCNTs induced angiogenesis, which was largely mediated by various fibrogenic mediators including p38 MAPK and ROS. Interestingly, a positive autocrine loop was observed between TGF-β1 and VEGF, which may exacerbate SWCNT-mediated cytotoxicity. In reporting SWCNT-induced angiogenesis, this study unveils an important physiological process associated with SWCNT-induced lung fibrosis. It is debatable that angiogenesis may either have a deleterious role, as is the case in cancer, or have an anti-fibrogenic role during the development of pulmonary fibrosis. This warrants further investigation in the field of angiogenesis related to pulmonary fibrosis in response to SWCNTs. Assessment of these effects *in vivo* will further substantiate the mechanisms involved in SWCNT-mediated pulmonary pathogenesis. Understanding the key mechanisms involved in SWCNT-mediated cytotoxicity will aid in the early detection and prevention of adverse health effects associated with SWCNT exposure.

Acknowledgements

This work was supported by grants from National Institutes of Health awarded to NA (1SC1-HL112630-01) and YR (R01-HL095579) and from National Science Foundation awarded to YR (EPS-1003907).

Declaration of interest

None of the authors has a financial relationship with a commercial entity that has an interest in the subject of this manuscript. The findings and conclusions in this report are those of the authors and do not necessarily represent the views of the National Institute for Occupational Safety and Health.

References

Beyaert R, Cuenda A, Vanden Berghe W, Plaisance S, Lee JC, Haegeman G, et al. 1996. The p38/RK mitogen-activated protein kinase pathway regulates interleukin-6 synthesis response to tumor necrosis factor. Embo J 15:1914–1923.

Brinckerhoff CE, Matrisian LM. 2002. Matrix metalloproteinases: a tail of a frog that became a prince. Nat Rev Mol Cell Biol 3:207–214.

Carmeliet P. 2000. Mechanisms of angiogenesis and arteriogenesis. Nat Med 6:389–395.

Clark RA, Mason RJ, Folkvord JM, Mcdonald JA. 1986. Fibronectin mediates adherence of rat alveolar type II epithelial cells via the fibroblastic cell-attachment domain. J Clin Invest 77:1831–1840.

Coker RK, Laurent GJ, Shahzeidi S, Lympany PA, Du Bois RM, Jeffery PK, et al. 1997. Transforming growth factors-beta 1, -beta 2, and -beta 3 stimulate fibroblast procollagen production in vitro but are differentially expressed during bleomycin-induced lung fibrosis. Am J Pathol 150:981–991.

Cosgrove GP, Brown KK, Schiemann WP, Serls AE, Parr JE, Geraci MW, et al. 2004. Pigment epithelium-derived factor in idiopathic pulmonary fibrosis: a role in aberrant angiogenesis. Am J Respir Crit Care Med 170:242–251.

Crouch E. 1990. Pathobiology of pulmonary fibrosis. Am J Physiol 259: L159–L184.

Daniels CE, Wilkes MC, Edens M, Kottom TJ, Murphy SJ, Limper AH, et al. 2004. Imatinib mesylate inhibits the profibrogenic activity of TGF-beta and prevents bleomycin-mediated lung fibrosis. J Clin Invest 114:1308–1316.

Demyanets S, Kaun C, Rychli K, Pfaffenberger S, Kastl SP, Hohensinner PJ, et al. 2011. Oncostatin M-enhanced vascular endothelial growth factor expression in human vascular smooth muscle cells involves PI3K-, p38 MAPK-, Erk1/2- and STAT1/STAT3-dependent pathways and is attenuated by interferon-gamma. Basic Res Cardiol 106:217–231.

Fehrenbach H, Kasper M, Haase M, Schuh D, Muller M. 1999. Differential immunolocalization of VEGF in rat and human adult lung, and in experimental rat lung fibrosis: light, fluorescence, and electron microscopy. Anat Rec 254:61–73.

Goldberg PL, Macnaughton DE, Clements RT, Minnear FL, Vincent PA. 2002. p38 MAPK activation by TGF-beta1 increases MLC phosphorylation and endothelial monolayer permeability. Am J Physiol Lung Cell Mol Physiol 282:L146–L154.

Han J, Lee JD, Bibbs L, Ulevitch RJ. 1994. A MAP kinase targeted by endotoxin and hyperosmolarity in mammalian cells. Science 265:808–811.

Helmlinger G, Endo M, Ferrara N, Hlatky L, Jain RK. 2000. Formation of endothelial cell networks. Nature 405:139–141.

Hiratsuka S, Duda DG, Huang Y, Goel S, Sugiyama T, Nagasawa T, et al. 2011. C-X-C receptor type 4 promotes metastasis by activating p38 mitogen-activated protein kinase in myeloid differentiation antigen (Gr-1)-positive cells. Proc Natl Acad Sci USA 108:302–307.

Huh JE, Nam DW, Baek YH, Kang JW, Park DS, Choi DY, et al. 2011. Formononetin accelerates wound repair by the regulation of early growth response factor-1 transcription factor through the phosphorylation of the ERK and p38 MAPK pathways. Int Immunopharmacol 11:46–54.

Inghilleri S, Morbini P, Oggionni T, Barni S, Fenoglio C. 2006. In situ assessment of oxidant and nitrogenic stress in bleomycin pulmonary fibrosis. Histochem Cell Biol 125:661–669.

Iordanov M, Bender K, Ade T, Schmid W, Sachsenmaier C, Engel K, et al. 1997. CREB is activated by UVC through a p38/HOG-1-dependent protein kinase. Embo J 16:1009–1022.

Kang HR, Lee CG, Homer RJ, Elias JA. 2007. Semaphorin 7A plays a critical role in TGF-beta1-induced pulmonary fibrosis. J Exp Med 204:1083–1093.

Keane MP, Arenberg DA, Lynch JP 3rd, Whyte RI, Iannettoni MD, Burdick MD, et al. 1997. The CXC chemokines, IL-8 and IP-10, regulate angiogenic activity in idiopathic pulmonary fibrosis. J Immunol 159:1437–1443.

Keane MP, Belperio JA, Arenberg DA, Burdick MD, Xu ZJ, Xue YY, et al. 1999a. IFN-gamma-inducible protein-10 attenuates bleomycin-induced pulmonary fibrosis via inhibition of angiogenesis. J Immunol 163:5686–5692.

Keane MP, Belperio JA, Burdick MD, Lynch JP, Fishbein MC, Strieter RM. 2001. ENA-78 is an important angiogenic factor in idiopathic pulmonary fibrosis. Am J Respir Crit Care Med 164:2239–2242.

Keane MP, Belperio JA, Moore TA, Moore BB, Arenberg DA, Smith RE, et al. 1999b. Neutralization of the CXC chemokine, macrophage inflammatory protein-2, attenuates bleomycin-induced pulmonary fibrosis. J Immunol 162:5511–5518.

Khalil N, Parekh TV, O'Connor R, Antman N, Kepron W, Yehaulaeshet T, et al. 2001. Regulation of the effects of TGF-beta 1 by activation of latent TGF-beta 1 and differential expression of TGF-beta receptors (T beta R-I and T beta R-II) in idiopathic pulmonary fibrosis. Thorax 56:907–915.

Kolosova I, Nethery D, Kern JA. 2011. Role of Smad2/3 and p38 MAP kinase in TGF-beta1-induced epithelial-mesenchymal transition of pulmonary epithelial cells. J Cell Physiol 226:1248–1254.

Lam CW, James JT, Mccluskey R, Hunter RL. 2004. Pulmonary toxicity of single-wall carbon nanotubes in mice 7 and 90 days after intratracheal instillation. Toxicol Sci 77:126–134.

Lu Y, Azad N, Wang L, Iyer AK, Castranova V, Jiang BH, et al. 2010. Phosphatidylinositol-3-kinase/akt regulates bleomycin-induced fibroblast proliferation and collagen production. Am J Respir Cell Mol Biol 42:432–441.

Mcanulty RJ, Laurent GJ. 1995. Pathogenesis of lung fibrosis and potential new therapeutic strategies. Exp Nephrol 3:96–107.

Meyer KC, Cardoni A, Xiang ZZ. 2000. Vascular endothelial growth factor in bronchoalveolar lavage from normal subjects and patients with diffuse parenchymal lung disease. J Lab Clin Med 135:332–338.

Moriguchi T, Toyoshima F, Gotoh Y, Iwamatsu A, Irie K, Mori E, et al. 1996. Purification and identification of a major activator for p38 from osmotically shocked cells. Activation of mitogen-activated protein kinase kinase 6 by osmotic shock, tumor necrosis factor-alpha, and H2O2. J Biol Chem 271:26981–26988.

Oberdorster G, Oberdorster E, Oberdorster J. 2005. Nanotoxicology: an emerging discipline evolving from studies of ultrafine particles. Environ Health Perspect 113:823–839.

Pandey P, Raingeaud J, Kaneki M, Weichselbaum R, Davis RJ, Kufe D, et al. 1996. Activation of p38 mitogen-activated protein kinase by c-Abl-dependent and -independent mechanisms. J Biol Chem 271:23775–23779.

Papakonstantinou E, Aletras AJ, Roth M, Tamm M, Karakiulakis G. 2003. Hypoxia modulates the effects of transforming growth factor-beta isoforms on matrix-formation by primary human lung fibroblasts. Cytokine 24:25–35.

Pardo A, Selman M. 2005. MMP-1: the elder of the family. Int J Biochem Cell Biol 37:283–288.

Peao MN, Aguas AP, De Sa CM, Grande NR. 1994. Neoformation of blood vessels in association with rat lung fibrosis induced by bleomycin. Anat Rec 238:57–67.

Pelton RW, Nomura S, Moses HL, Hogan BL. 1989. Expression of transforming growth factor beta 2 RNA during murine embryogenesis. Development 106:759–767.

Quinlan T, Spivack S, Mossman BT. 1994. Regulation of antioxidant enzymes in lung after oxidant injury. Environ Health Perspect 102 (Suppl 2):79–87.

Raingeaud J, Gupta S, Rogers JS, Dickens M, Han J, Ulevitch RJ, et al. 1995. Pro-inflammatory cytokines and environmental stress cause p38 mitogen-activated protein kinase activation by dual phosphorylation on tyrosine and threonine. J Biol Chem 270:7420–7426.

Renzoni EA, Walsh DA, Salmon M, Wells AU, Sestini P, Nicholson AG, et al. 2003. Interstitial vascularity in fibrosing alveolitis. Am J Respir Crit Care Med 167:438–443.

Roberts AB, Sporn MB, Assoian RK, Smith JM, Roche NS, Wakefield LM, et al. 1986. Transforming growth factor type beta: rapid induction of fibrosis and angiogenesis in vivo and stimulation of collagen formation in vitro. Proc Natl Acad Sci USA 83:4167–4171.

Roos TU, Heiss EH, Schwaiberger AV, Schachner D, Sroka IM, Oberan T, et al. 2011. Caffeic acid phenethyl ester inhibits PDGF-Induced proliferation of vascular smooth muscle cells via activation of p38 MAPK, HIF-1alpha, and Heme Oxygenase-1. J Nat Prod 74:352–356.

Selman M, King TE, Pardo A. 2001. Idiopathic pulmonary fibrosis: prevailing and evolving hypotheses about its pathogenesis and implications for therapy. Ann Intern Med 134:136–151.

Selman M, Montano M, Ramos C, Chapela R. 1986. Concentration, biosynthesis and degradation of collagen in idiopathic pulmonary fibrosis. Thorax 41:355–359.

Shields KM, Panzhinskiy E, Burns N, Zawada WM, Das M. 2011. Mitogen-activated protein kinase phosphatase-1 is a key regulator of hypoxia-induced vascular endothelial growth factor expression and vessel density in lung. Am J Pathol 178:98–109.

Shvedova AA, Kagan VE. 2010. The role of nanotoxicology in realizing the 'helping without harm' paradigm of nanomedicine: lessons from studies of pulmonary effects of single-walled carbon nanotubes. J Intern Med 267:106–118.

Shvedova AA, Kisin E, Murray AR, Johnson VJ, Gorelik O, Arepalli S, et al. 2008. Inhalation vs. aspiration of single-walled carbon nanotubes in C57BL/6 mice: inflammation, fibrosis, oxidative stress, and mutagenesis. Am J Physiol Lung Cell Mol Physiol 295: L552–L565.

Shvedova AA, Kisin ER, Mercer R, Murray AR, Johnson VJ, Potapovich AI, et al. 2005. Unusual inflammatory and fibrogenic pulmonary responses to single-walled carbon nanotubes in mice. Am J Physiol Lung Cell Mol Physiol 289:L698–L708.

Sorensen V, Zhen Y, Zakrzewska M, Haugsten EM, Walchli S, Nilsen T, et al. 2008. Phosphorylation of fibroblast growth factor (FGF) receptor 1 at Ser777 by p38 mitogen-activated protein kinase regulates translocation of exogenous FGF1 to the cytosol and nucleus. Mol Cell Biol 28:4129–4141.

Steurer M, Zoller H, Augustin F, Fong D, Heiss S, Strasser-Weippl K, et al. 2007. Increased angiogenesis in chronic idiopathic myelofibrosis: vascular endothelial growth factor as a prominent angiogenic factor. Hum Pathol 38:1057–1064.

Thannickal VJ, Toews GB, White ES, Lynch JP 3rd, Martinez FJ. 2004. Mechanisms of pulmonary fibrosis. Annu Rev Med 55:395–417.

Turner-Warwick M. 1963. Precapillary Systemic-Pulmonary Anastomoses. Thorax 18:225–237.

Wang L, Castranova V, Mishra A, Chen B, Mercer RR, Schwegler-Berry D, et al. 2010a. Dispersion of single-walled carbon nanotubes by a natural lung surfactant for pulmonary in vitro and in vivo toxicity studies. Part Fibre Toxicol 7:31.

Wang L, Mercer RR, Rojanasakul Y, Qiu A, Lu Y, Scabilloni JF, et al. 2010b. Direct fibrogenic effects of dispersed single-walled carbon nanotubes on human lung fibroblasts. J Toxicol Environ Health A 73:410–422.

Warheit DB, Laurence BR, Reed KL, Roach DH, Reynolds GA, Webb TR. 2004. Comparative pulmonary toxicity assessment of single-wall carbon nanotubes in rats. Toxicol Sci 77:117–125.

Xiong S, Grijalva R, Zhang L, Nguyen NT, Pisters PW, Pollock RE, et al. 2001. Up-regulation of vascular endothelial growth factor in breast cancer cells by the heregulin-beta1-activated p38 signaling pathway enhances endothelial cell migration. Cancer Res 61: 1727–1732.

Xu YD, Hua J, Mui A, O'Connor R, Grotendorst G, Khalil N. 2003. Release of biologically active TGF-beta1 by alveolar epithelial cells results in pulmonary fibrosis. Am J Physiol Lung Cell Mol Physiol 285:L527–L539.

Yang EY, Moses HL. 1990. Transforming growth factor beta 1-induced changes in cell migration, proliferation, and angiogenesis in the chicken chorioallantoic membrane. J Cell Biol 111:731–741.

Zhang P, Xu D, Wang S, FU H, Wang K, Zou Y, et al. 2011. Inhibition of aldehyde dehydrogenase 2 activity enhances antimycin-induced rat cardiomyocytes apoptosis through activation of MAPK signaling pathway. Biomed Pharmacother 65(8):590–593.